NANO LETTERS

Letter

pubs.acs.org/NanoLett

Thermally Driven Crossover from Indirect toward Direct Bandgap in 2D Semiconductors: $MoSe_2$ versus MoS_2

Sefaattin Tongay,*[,†] Jian Zhou,[†] Can Ataca,[‡] Kelvin Lo,[†] Tyler S. Matthews,[†] Jingbo Li,[§] Jeffrey C. Grossman,[‡] and Junqiao Wu*[,†,∥]

[†]Department of Materials Science and Engineering, University of California, Berkeley, California 94720, United States

[‡]Department of Materials Science and Engineering, Massachusetts Institute of Technology, Cambridge, Massachusetts 02139, United States

[§]Institute of Semiconductors, Chinese Academy of Sciences, P.O. Box 912, Beijing 100083, People's Republic of China

[∥]Materials Sciences Division, Lawrence Berkeley National Laboratory, Berkeley, California 94720, United States

Supporting Information

ABSTRACT: Layered semiconductors based on transition-metal chalcogenides usually cross from indirect bandgap in the bulk limit over to direct bandgap in the quantum (2D) limit. Such a crossover can be achieved by peeling off a multilayer sample to a single layer. For exploration of physical behavior and device applications, it is much desired to reversibly modulate such crossover in a multilayer sample. Here we demonstrate that, in a few-layer sample where the indirect bandgap and direct bandgap are nearly degenerate, the temperature rise can effectively drive the system toward the 2D limit by thermally decoupling neighboring layers via interlayer thermal expansion. Such a situation is realized in few-layer $MoSe_2$, which shows stark contrast from the well-explored MoS_2 where the indirect and direct bandgaps are far from degenerate. Photoluminescence of few-layer $MoSe_2$ is much enhanced with the temperature rise, much like the way that the photoluminescence is enhanced due to the bandgap crossover going from the bulk to the quantum limit, offering potential applications involving external modulation of optical properties in 2D semiconductors. The direct bandgap of $MoSe_2$, identified at 1.55 eV, may also promise applications in energy conversion involving solar spectrum, as it is close to the optimal bandgap value of single-junction solar cells and photoelechemical devices.

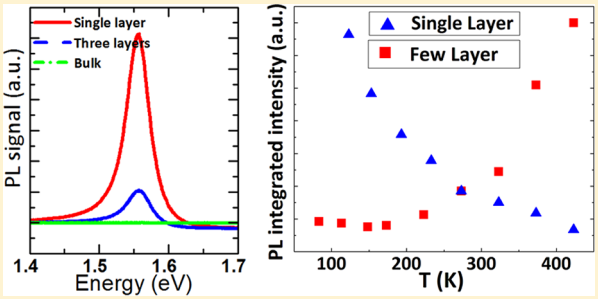

KEYWORDS: *2D-Semiconductors, $MoSe_2$, MoS_2, photoluminescence, bandgap, temperature dependence*

Two-dimensional (2D) materials have attracted much interest mainly owing to their exotic physical properties that are strikingly different from their three-dimensional (bulk) counterparts. Even though graphene, the most famous member of the 2D material family, possesses extraordinary properties[1] and is readily integrated in various applications,[2−4] the lack of a native bandgap in graphene has led to a broad search for other 2D semiconducting materials. More recently, the transition-metal dichalcogenide (TMD) semiconductor MoS_2 has been focused on and has shown great potential in the field; single-layer MoS_2 has been used as an integral part of transistors,[5−8] sensors,[9] and magnetic materials.[10] However, beyond MoS_2, other layered TMDs offer a large variety of 2D materials with distinct properties.

In this work we studied, for the first time, single-layer $MoSe_2$ mechanically exfoliated onto SiO_2/Si.[11] Single-layer $MoSe_2$ displays good thermal stability with a 1.55 eV direct bandgap as determined from photoluminescence (PL) measurements. The PL peak intensity is enhanced dramatically from few-layer to single-layer as a result of the crossover from indirect bandgap in the bulk limit to direct bandgap in the quantum (2D) limit, similar to the behavior of MoS_2.[12−14] More interestingly, we find that few-layer $MoSe_2$ flakes posssess a nearly degenerate indirect and direct bandgap, and an increase in temperature can effectively push the system toward the quasi-2D limit by thermally reducing the coupling between the layers. This response in few-layer $MoSe_2$ is similar to the enhancement in PL due to the crossover from indirect to direct bandgap originating from the quantum confinement effect. In this regard, $MoSe_2$ shows stark differences from MoS_2 where not only the bandgap value is higher than in $MoSe_2$, but also the indirect and direct bandgaps are well-separated in energy and hence far from degenerate. Our results not only introduce single-layer $MoSe_2$ as a new 2D material with a bandgap well matched to the solar spectrum, but also open up a new direction for 2D applications where external modulation of bandgap and optical properties is desired.

Received: July 12, 2012
Revised: October 23, 2012
Published: October 25, 2012

   dx.doi.org/10.1021/nl302584w | *Nano Lett.* 2012, 12, 5576−5580

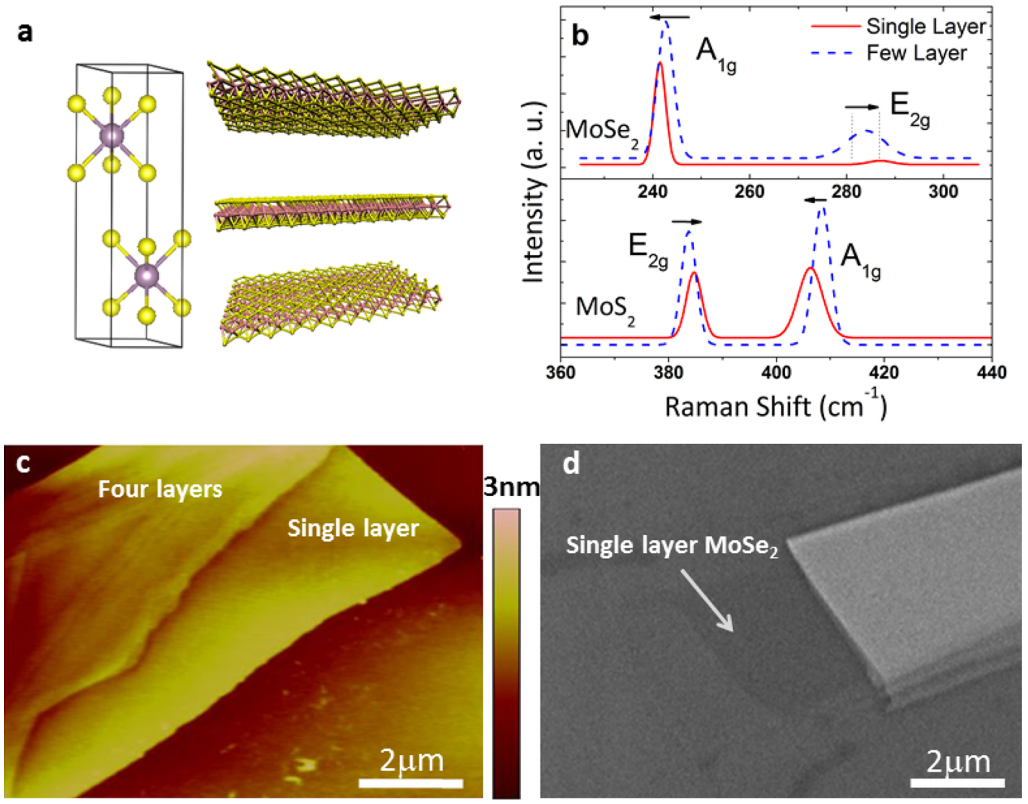

Figure 1. (a) Crystal structure of $MoSe_2$ in the bulk (2H-$MoSe_2$). (b) Raman spectrum of single (solid red line) and more than 10 layers (dashed blue line) MoX_2 (X = S, Se). (c) AFM image taken on a single-layer $MoSe_2$ flake. (d) SEM image taken on a $MoSe_2$ flake.

Single and few-layer MoS_2 and $MoSe_2$ flakes were exfoliated from bulk MoS_2 and $MoSe_2$ crystals onto 90 nm SiO_2/Si substrates using a conventional mechanical exfoliation technique[11] (see Supporting Information). 90 nm SiO_2/Si substrates allowed us to improve the contrast between MoX_2 (X = S, Se) layers and at the same time increased the visibility of the single layer sheets.[15] Exfoliated few-layer flakes have shown characteristic A_{1g} (out-of-plane) and E^1_{2g} (in-plane) Raman modes (Figure 1b) located at 243.0 and 283.7 cm^{-1} for $MoSe_2$ and 408.7 and 383.7 cm^{-1} for MoS_2. For $MoSe_2$, the A_{1g} mode is at a higher frequency than E_{2g} mode, consistent with earlier studies.[16−18] We find that the peak position of these Raman modes show a slight dependence on the layer thickness. In the single layer limit, the A_{1g} Raman mode softens to 241.2 (406.1) cm^{-1} as the E^1_{2g} mode stiffens to 287.3 (384.7) cm^{-1} for $MoSe_2$ (MoS_2). Since interlayer coupling is absent in the single layer limit, the out-of-plane A_{1g} mode is expected to soften as a result of reduction of the restoring forces arising from the absence of interlayer coupling. However this model does not account for the stiffening of the in-plane E^1_{2g} mode.[19] More interestingly, the intensity ratio between the A_{1g} and E^1_{2g} modes ($I_{A_{1g}}/I_{E^1_{2g}}$) changes from 4.9 for few-layer (∼10 layers) to 23.1 for the single-layer $MoSe_2$, while the ratio remains nearly a constant (∼1.2) in the MoS_2 case. In Figure 1c−d, we display AFM and SEM images taken on a single-layer $MoSe_2$. The single layers typically display 0.9−1 nm thickness in the AFM contact mode, and the surface is free of residues. Also, these single layers are readily visible on 90 nm SiO_2/Si under the scanning electron microscope as shown in Figure 1d.

In the bulk limit, $MoSe_2$ is an indirect bandgap semiconductor with a 1.1 eV bandgap value,[20] and therefore the bandgap PL is expected to be rather weak. However, the few-layer $MoSe_2$ flakes show gradual enhancement in PL intensity at around 1.5−1.6 eV, and the PL peak intensity reaches its maximum value for a single-layer $MoSe_2$ as shown in Figure 2a. Similar to this observation, enhancement in PL for single-layer

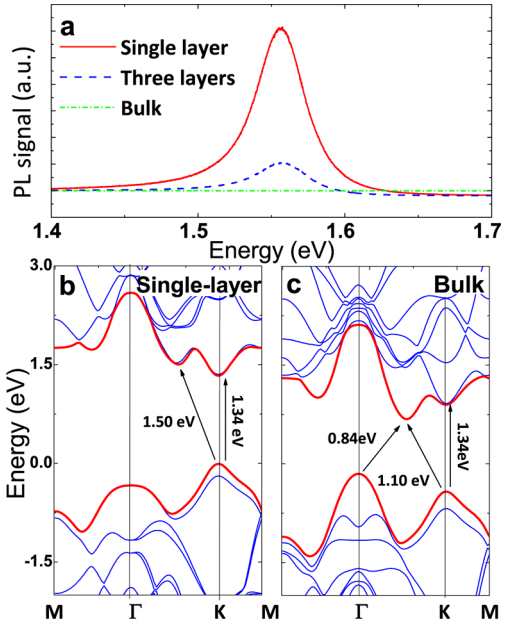

Figure 2. (a) Measured room-temperature photoluminescence on a single-layer (red), three-layer (blue dashed), and bulk (green dotted dashed) $MoSe_2$. Here the measurement parameters including laser excitation intensity are the same. (b−c) Calculated band structure of single-layer and bulk $MoSe_2$.

dx.doi.org/10.1021/nl302584w | *Nano Lett.* 2012, 12, 5576−5580

MoS_2 has been observed previously[12−14] and attributed to an indirect-to-direct bandgap crossover associated with the quantum confinement in the perpendicular direction.[13] To confirm this, we compute the electronic band structure of single-layer $MoSe_2$ and bulk $MoSe_2$ in Figure 2b−c calculated by generalized gradient approximatio (GGA) + van der Waals (vdW) + spin−orbit density functional theory (see Supporting Information, Figure 3a−b). Here, three-dimensional MoX_2 ($2H\text{-}MoX_2$) possesses both time-reversal and inversion symmetry, and therefore spin-up and spin-down valence bands are degenerate. Upon lowering the dimensionality of the system to single layer (1H-), the inversion symmetry is lost, and the degeneracy is lifted due to spin−orbit interaction. It is therefore necessary to take into account the spin−orbit coupling interaction in density functional theory (DFT) calculations to determine the accurate band structure. We also note that the first principles calculations typically underestimate the actual bandgap, leading to small discrepancies from the experimental values. In accord with the above discussions, bulk $MoSe_2$ displays 0.84 eV Γ to Γ−K, 1.10 eV K to Γ−K an indirect bandgaps, and a 1.34 eV K−K direct bandgap (Figure 2c). In contrast, for single-layer $MoSe_2$, Γ to Γ−K and K to Γ−K increases, while the K−K direct gap remains nearly unchanged and $MoSe_2$ becomes a direct bandgap semiconductor with a 1.34 eV bandgap value at the K symmetry point (Figure 2b). Even though the band structure calculations explain the enhancement in PL in the quantum confinement limit, it does not address the origin of the weaker PL peak observed for few-layer flakes. In fact, our calculations show that two and three layer $MoSe_2$ have an indirect bandgap but with almost degenerate direct and indirect bandgap values (Figure 4a−b).[21] In such a case, hot carriers are expected to transiently occupy the available states around the K symmetry point and result in hot PL although with weaker intensity compared to the single layer case (Figure 2a). This hot PL model was invoked and justified by Mak et al.[13] to explain the weak PL in few-layer MoS_2. The hot PL effect is expected to be stronger in $MoSe_2$ due to the closer values of direct and indirect bandgaps.

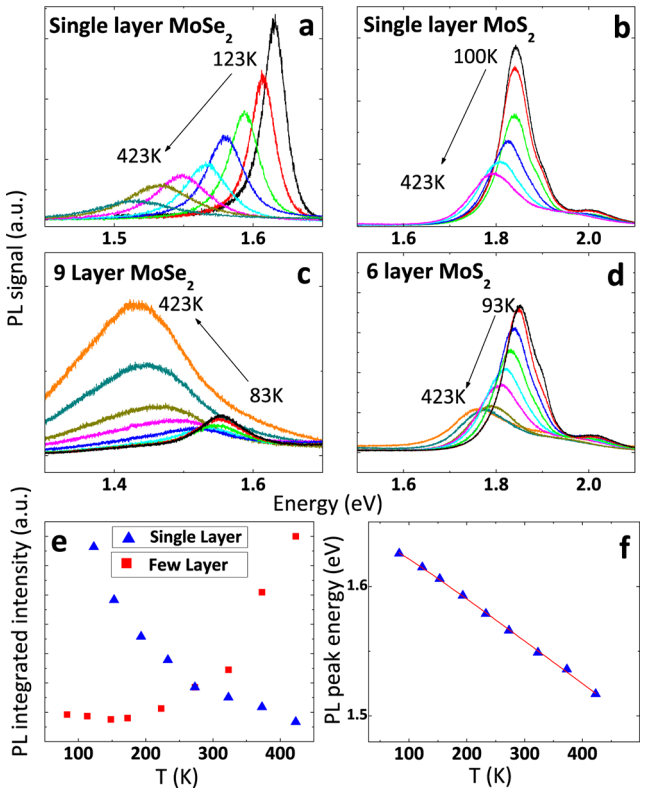

Figure 3. Temperature dependence of photoluminescence on (a−b) single-layer $MoSe_2$ and MoS_2 and (c−d) few-layer $MoSe_2$ and MoS_2. Here, the PL intensity ratio between the single-layer and few-layer MoX_2 typically reaches 50−500. (e) Temperature dependence of photoluminescence intensity measured on a single-layer (blue triangles) and nine-layer (red squares) $MoSe_2$ flakes. (f) Variation of the single-layer $MoSe_2$ bandgap values (PL peak energy) in the 87−450 K range. The red line shows the fitting results using 1.

Before presenting striking differences between single and few-layer $MoSe_2$ and MoS_2, we emphasize that the bandgap (PL peak position) of single-layer $MoSe_2$ is located at 1.55 eV, where this value is near 1.9 eV for single-layer MoS_2. Moreover, heating single-layer $MoSe_2$ in air to 500 K, the maximum temperature that can be attained in our system, does not alter its PL peak intensity and position upon cooling back to room temperature, implying that the single layers are thermally stable up to these temperatures. Previously, the oxidization characteristics of bulk MoS_2 and $MoSe_2$ have been studied, and they were found to be oxidized in the 500−700 K range.[22,23] However, considering that the studied flakes are two-dimensional, the observed stability is surprising. This might be due to self-limited oxidization and merits further studies. The observed bandgap value is significantly smaller than that of MoS_2, and this not only extends the bandgap values observed in 2D semiconductors but also points to creating a range of bandgap values by alloying 2D semiconductors. More importantly, the 1.55 eV direct bandgap in $MoSe_2$ is more relevant to device applications involving the solar spectrum, as it is near the optimal bandgap value for single-junction solar cells and photoelectrochemical cells.

Next, we turn our attention to the temperature dependence of PL measured on single- and few-layer samples of $MoSe_2$ and MoS_2 (Figure 3a−d). Such measurements not only yield the bandgap dependence on temperature but also allow us to understand the physical mechanism that governs the light emission process. Before discussing the effect of temperature on the bandgap (E_g), we focus on the change in PL intensity as a function of temperature. As seen in Figure 3a−c, the temperature dependence of PL intensity of the single-layer and few-layer $MoSe_2$ show striking differences. While the PL intensity is much reduced at high temperatures for single-layer $MoSe_2$, it is surprisingly enhanced for few-layer $MoSe_2$. Generally the PL of semiconductors decreases in intensity as the PL peak broadens with increasing temperature. The suppression in PL intensity and peak broadening are typically attributed to the exponential enhancement in nonradiative electron−hole recombination processes, reducing the probability of radiative transition. Even though this model applies well to single-layer $MoSe_2$, it fails for the few-layer $MoSe_2$ samples where the PL intensity is enhanced at high temperatures (see Figure 3e, red squares). We also employed similar measurements on a single-layer and few-layer MoS_2 flakes in the same temperature window, and we have found that the PL intensity of MoS_2 decreases at high temperatures regardless of the layer thickness (Figure 3b and d)[24] just like in the case of single-layer $MoSe_2$ and other conventional semiconductors. The distinct difference in the temperature

dx.doi.org/10.1021/nl302584w | Nano Lett. 2012, 12, 5576−5580

behavior of these two materials points out to intrinsic differences in their band structure.

To gain further insight, we compare the band structures of $MoSe_2$ and MoS_2 from bulk to few-layer and to the single-layer limit. According to our DFT calculations as well as previously reported studies on $MoSe_2$ and MoS_2,[21,25] these two materials possess indirect bandgap in bulk and become direct bandgap in the 2D limit. Therefore in those limits, one would expect $MoSe_2$ and MoS_2 to behave similarly. However, we find that the rate of the indirect-to-direct bandgap crossover differs significantly between MoS_2 and $MoSe_2$. Even though single-layer $MoSe_2$ is a direct bandgap semiconductor (1.34 eV), the indirect bandgap value (1.50 eV) lies close to the direct bandgap. This difference of 0.16 eV is much smaller than the difference of 0.35 eV between the direct (1.54 eV) and indirect (1.89 eV) bandgap of single-layer MoS_2. As the number of layers increases, the quantum confinement in the perpendicular direction is relaxed, and therefore the indirect bandgap value becomes smaller, while the direct bandgap value remains largely unchanged, due mostly to the heavier effective mass associated with the *K* symmetry point (see Supporting Information, Figures 3 and 4). During this crossover the direct and indirect gaps in the case of bilayer and few-layer $MoSe_2$ becomes nearly degenerate. An increase in temperature slightly expands the interlayer distance as evidenced by the temperature-dependent Raman measurements (see Supporting Information) and tends to decouple neighboring $MoSe_2$ layers, pushing the system further toward the bandgap degeneracy. In this case, the contribution from the hot PL across the direct bandgap to the PL intensity becomes much stronger at high temperatures without any need for a phonon-assisted process. The abnormal increase in PL intensity at high temperatures, on the other hand, cannot be attributed to Boltzmann tailing of equilibrium electrons populating the conduction and valence bands at the *K* point where the direct bandgap occurs. This is because this *K* point bandgap is still 0.18 eV above the indirect bandgap which is much larger than k_BT. In a 3D semiconductor with similar band configuration, Ge, the direct bandgap is 0.14 eV above the indirect bandgap, but such an unusual PL behavior as in $MoSe_2$ has never been observed in Ge. This contrast highlights the uniqueness of 2D semiconductors that they support a high-efficiency hot PL process.

Shown in Figure 4 is the calculated bandgap crossover of few-layer $MoSe_2$ MoS_2 as a function of modulation in interlayer distance. Here, the relaxed equilibrium position is fixed to zero, and additional layer spacing (abscissa) imitates the effect of temperature rise on the interlayer coupling. As seen from the figure, at the equilibrium, the indirect bandgap (Γ to Γ−K) defines the fundamental bandgap but is close in value to the direct band (K to K). Increasing the interlayer spacing reduces the coupling between the layers and leads to an increase in Γ to Γ−K gap, while the direct gap K−K remains unchanged. During this transition, the indirect and direct bandgaps in bilayer and trilayer $MoSe_2$ would become degenerate as discussed above. For larger interlayer spacing, the coupling would be weakened to a point that individual layers in the few-layer system start to behave as single layers with a 1.34 eV direct bandgap. On the contrary, since the indirect and direct gaps are well-separated in the bilayer MoS_2, band degeneracy cannot be thermally approached unless the layers are physically decoupled from each other. This distinct difference between these two similar materials leads to a drastic difference in the temperature dependence of their PL intensity.

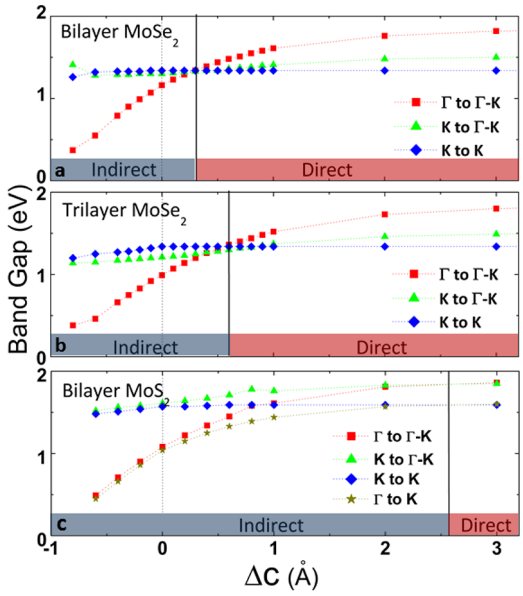

Figure 4. Variation of the bandgap values between different symmetry points as a function of layer spacing on (a) bilayer $MoSe_2$, (b) trilayer $MoSe_2$, and (c) bilayer MoS_2. A fully relaxed (equilibrium) position is fixed to zero, and additional layer spacing (abscissa) imitates the effect of temperature on the interlayer coupling.

Since this is the first experimental observation of single-layer $MoSe_2$, for completeness, we discuss the effect of temperature on the bandgap (PL peak position) of the single-layer $MoSe_2$. In Figure 3f, we show the temperature dependence of the bandgap extracted out from Figure 3a. The observed decrease in the bandgap as a function of temperature is very similar to that observed in conventional semiconductors where such a decrease at higher temperatures due to increased electron−phonon interactions as well as slight changes in the bonding length.[26] Even though the origin of the temperature dependence in E_g is known, a physically meaningful and accurate formula of $E_g(T)$ is lacking. Often times, the temperature dependence is fitted by the emprical Varshni relation[27] where the parameters lack clear physical meaning. Here, we employ a semiempirical fitting function;[28]

$$E_g(T) = E_g^0 - S\langle\hbar\omega\rangle[\cosh(\langle\hbar\omega\rangle/2k_BT) - 1] \quad (1)$$

where E_g^0 is the zero-temperature bandgap value, *S* is a parameter describing the strength of the electron−phonon coupling, $<\hbar\omega>$ is the average acoustic phonon energy involving in the electron−phonon interaction, and last the cosh term is related to the density of phonons at the specific temperature. We find that this model fits the temperature dependence of the bandgap well as shown in Figure 3f with E_g^0 = 1.64 eV, S = 1.93, and $<\hbar\omega\geq$11.6 meV (93 cm^{-1}). In comparison, similar fitting to single-layer MoS_2 yields E_g^0 = 1.86 eV, S = 1.82, and $\langle\hbar\omega\rangle$ = 22.5 meV (182 cm^{-1}).

To summarize, we have experimentally shown the first optical emission studies of single-layer and few-layer $MoSe_2$ semiconductors. While single-layer $MoSe_2$ possesses a direct bandgap, in the few-layer limit the indirect and direct bandgap are nearly degenerate. As a result, we find that this system can be effectively driven toward the 2D limit by thermally decoupling neighboring layers via interlayer thermal expansion. This finding leads to an enhancement in photoluminescence of few-layer $MoSe_2$ at high temperatures, similar to the enhance-

dx.doi.org/10.1021/nl302584w | *Nano Lett.* 2012, 12, 5576−5580

ment of photoluminescence due to the bandgap crossover going from the bulk to the quantum limit. However, observed temperature dependence of the PL in few-layer $MoSe_2$ is strikingly different from the well-explored MoS_2 where the indirect and direct bandgaps are far from degenerate. This effect points to potential applications involving external modulation of optical properties in 2D semiconductors.

Methods. *Experimental Details.* Raman and photoluminescence measurements were performed using a Renishaw Raman system with 488 nm laser in combination with commercially available liquid N_2 cooling stage. Typically, samples were measured using 100× lens, and the laser beam was focused on a ∼1 μm diameter spot. Atomic force microscopy measurements were performed using a commercial system (Multimode, Veeco). The imaging and thickness measurements have been done with both contact mode and tapping mode.

See Supporting Information for the $MoSe_2$ single crystal growth process. MoS_2 single crystals were purchased from SPI Inc. and 2Dsemiconductors.com. See the Supporting Information for more on sample preperation.

Density Functional Theory Calculations. Our calculations are based on first-principles density functional theory (DFT) using projector augmented wave potentials.[29] The exchange correlation potential has been represented by the generalized gradient approximation characterized by Perdew–Burke–Ernzerhof[30] including van der Waals (vdW) corrections[31] both for spin-polarized and spin-unpolarized cases. Effects of spin–orbit coupling and noncollinear magnetism are taken into account in the spin-polarized calculations. The supercell size, kinetic energy cutoff, and Brillouin zone (BZ) sampling of the calculations have been determined after extensive convergence analyses. A large spacing of ∼15 Å between 2D single layers is used to prevent interlayer interactions. A plane-wave basis set with kinetic energy cutoff of 300 eV is used. In the self-consistent field potential and total energy calculations the BZ is sampled by special **k**-points. The numbers of these **k**-points are $(25 \times 25 \times 1)$ and $(15 \times 15 \times 5)$ for the primitive 1H-MoS_2 and 2H-MoS_2 unit cell and are scaled according to the size of the super cells. All atomic positions and lattice constants are optimized using the conjugate gradient method, where the total energy and atomic forces are minimized. The convergence for energy is chosen as 10^{-6} eV between two consecutive steps, and the maximum Hellmann–Feynman forces acting on each atom is less than 0.01 eV/Å upon ionic relaxation. The pressure in the unit cell is kept below 5 kbar. Numerical calculations have been performed by using VASP software.[32] Frequencies of phonon modes are calculated using small displacement method (SDM)[33] in terms of forces calculated from first-principles.

■ ASSOCIATED CONTENT

Supporting Information

Sample preparation methods and additional information on the DFT calculations and Raman peaks. This material is available free of charge via the Internet at http://pubs.acs.org.

■ AUTHOR INFORMATION

Corresponding Author

*E-mail: tongay@berkeley.edu; wuj@berkeley.edu.

Notes

The authors declare no competing financial interest.

■ ACKNOWLEDGMENTS

This work was supported by the U.S. Department of Energy Early Career Award DE-FG02-11ER46796. The materials preparation part was supported by the Office of Science, Office of Basic Energy Sciences, of the U.S. Department of Energy under Contract No. DE-AC02-05CH11231.

■ REFERENCES

(1) Castro Neto, A. H.; Guinea, F.; Peres, N. M. R.; Novoselov, K. S.; Geim, A. K. *Rev. Mod. Phys.* **2009**, *81*, 109–162.
(2) Wu, Y.; Lin, Y. M.; Bol, A. A.; Jenkins, K. A.; Xia, F.; Farmer, D. B.; Zhu, Y.; Avouris, P. *Nature* **2011**, *472*, 74–78.
(3) Miao, X.; Tongay, S.; Petterson, M. K.; Berke, K.; Rinzler, A. G.; Appleton, B. R.; Hebard, A. F. *Nano Lett.* **2012**, *12*, 2745–2750.
(4) Zhang, B.; Cui, T. *Appl. Phys. Lett.* **2011**, *98*, 073116.
(5) Radisavljevic, B.; Radenovic, A.; Brivio, J.; Giacometti, V.; Kis, A. *Nat. Nanotechnol.* **2011**, *6*, 147–150.
(6) Zhang, Y.; Ye, J.; Matsuhashi, Y.; Iwasa, Y. *Nano Lett.* **2012**, *12*, 1136–1140.
(7) Lui, H.; Ye, P. *IEEE Electron Device Lett.* **2012**, *33*, 546–548.
(8) Yin, Z.; Li, H.; Li, H.; Jiang, L.; Shi, Y.; Sun, Y.; Lu, G.; Zhang, Q.; Chen, X.; Zhang, H. *ACS Nano* **2012**, *6*, 74–80.
(9) Li, H.; Yin, Z.; He, Q.; Li, H.; Huang, X.; Lu, G.; Fam, D. W. H.; Tok, A. I. Y.; Zhang, Q.; Zhang, H. *Small* **2012**, *8*, 63–67.
(10) Tongay, S.; Varnoosfaderan, S. S.; B. R. Appleton, J. W.; Hebard, A. F. *Appl. Phys. Lett.* **2012**, *101*, 123105.
(11) Novoselov, K. S.; Geim, A. K.; Morozov, S. V.; Jiang, D.; Zhang, Y.; Dubonos, S. V. *Science* **2004**, *306*, 666–669.
(12) Splendiani, A.; Sun, L.; Zhang, Y.; Li, T.; Kim, J.; Chim, C.-Y.; Galli, G.; Wang, F. *Nano Lett.* **2010**, *10*, 1271–1275 ; PMID: 20229981.
(13) Mak, K. F.; Lee, C.; Hone, J.; Shan, J.; Heinz, T. F. *Phys. Rev. Lett.* **2010**, *105*, 136805.
(14) Eda, G.; Yamaguchi, H.; Voiry, D.; Fujita, T.; Chen, M.; Chhowalla, M. *Nano Lett.* **2011**, *11*, 5111–5116.
(15) Benameur, M. M.; Radisavljevic, B.; Sahoo, J. S. H.; Berger, H.; Kis, A. *Nanotechnology* **2011**, *22*, 125706.
(16) Sugai, S.; Ueda, T. *Phys. Rev. B* **1982**, *26*, 6554.
(17) Lee, C.; Yan, H.; Brus, L. E.; Heinz, T. F.; Hone, J.; Ryu, S. *ACS Nano* **2010**, *4*, 2695–2700 ; PMID: 20392077.
(18) Sekine, T.; Izumi, M.; Nakashizu, T.; Uchinokura, K.; Matsuura, E. *J. Phys. Soc. Jpn.* **1980**, *49*, 1069–1077.
(19) Chakraborty, B.; Bera, A.; Muthu, D. V. S.; Bhowmick, S.; Waghmare, U. V.; Sood, A. K. *Phys. Rev. B* **2012**, *85*, 161403.
(20) Scheer, R.; Schock, H.-W. *Chalcogenide Photovoltaics: Physics, Technologies, and Thin Film Devices*; Wiley-VCH Verlag GmbH & Co.: Weinheim, Germany, 2011.
(21) Yun, W. S.; Han, S. W.; Hong, S. C.; Kim, I. G.; Lee, J. D. *Phys. Rev. B* **2012**, *85*, 033305.
(22) Moore, G. D. *ASLE Trans.* **1970**, *13* (2), 117–126.
(23) Lavik, M. T.; M., G. D.; Medved, T. M. *ASLE Trans.* **1968**, *11*, 44–55.
(24) Korn, T.; Heydrich, S.; Hirmer, M.; Schmutzler, J.; Schuller, C. *Appl. Phys. Lett.* **2011**, *99*, 102109.
(25) Ataca, C.; Sahin, H.; Ciraci, S. *J. Phys. Chem. C* **2012**, *116*, 8983–8999.
(26) Yu, P.; Cardona, M. *Fundamentals of Semiconductors: Physics and Materials Properties*; Springer: New York, 1999.
(27) Sze, S. M. *Physics of Semiconductor Devices*; John Wiley and Sons: New York, 1981.
(28) O'Donnell, K. P.; Chen, X. *Appl. Phys. Lett.* **1991**, *58*, 2924–2926.
(29) Blöchl, P. E. *Phys. Rev. B* **1994**, *50*, 17953–17979.
(30) Perdew, J. P.; Burke, K.; Ernzerhof, M. *Phys. Rev. Lett.* **1996**, *77*, 3865–3868.
(31) Grimme, S. *J. Comput. Chem.* **2006**, *27*, 1787.
(32) Kresse, G.; Hafner, J. *Phys. Rev. B* **1993**, *47*, 558–561.
(33) Alfe, D. *Phys. Commun.* **2009**, *180*, 2622.